

Shaking the Fake: Detecting Deepfake Videos in Real Time via Active Probes

Jun Luo

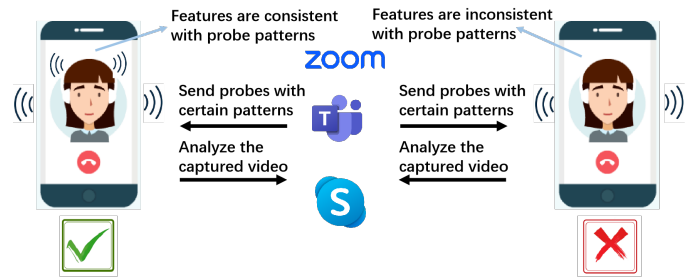
Nanyang Technological University, Singapore

Email: {zhixin001, junluo}@ntu.edu.sg

Abstract—Real-time deepfake, a type of generative AI, is capable of “creating” non-existing contents (e.g., swapping one’s face with another) in a video. It has been, very unfortunately, misused to produce deepfake videos (during web conferences, video calls, and identity authentication) for malicious purposes, including financial scams and political misinformation. Deepfake detection, as the countermeasure against deepfake, has attracted considerable attention from the academic community, yet existing works typically rely on learning *passive* features that may perform poorly beyond seen datasets. In this paper, we propose SFake, a new real-time deepfake detection method that innovatively exploits deepfake models’ inability to adapt to physical interference. Specifically, SFake *actively* sends probes to trigger mechanical vibrations on the smartphone, resulting in *the controllable* feature on the footage. Consequently, SFake determines whether the face is swapped by deepfake based on the consistency of the facial area with the probe pattern. We implement SFake, evaluate its effectiveness on a self-built dataset, and compare it with six other detection methods. The results show that SFake outperforms other detection methods with higher detection accuracy, faster process speed, and lower memory consumption.

1. Introduction

Real-time deepfake detection is a challenging task due to the high similarity between real and fake faces. Existing methods typically rely on learning passive features that may perform poorly beyond seen datasets. In this paper, we propose SFake, a new real-time deepfake detection method that innovatively exploits deepfake models’ inability to adapt to physical interference. Specifically, SFake actively sends probes to trigger mechanical vibrations on the smartphone, resulting in the controllable feature on the footage. Consequently, SFake determines whether the face is swapped by deepfake based on the consistency of the facial area with the probe pattern. We implement SFake, evaluate its effectiveness on a self-built dataset, and compare it with six other detection methods. The results show that SFake outperforms other detection methods with higher detection accuracy, faster process speed, and lower memory consumption.



real-time deepfake

mobile devices

passively

passively

can the detector actively introduce changes (or features) into videos that are i) controllable, ii) readily recognizable, and iii) affect the real and fake parts in a video distinctively?

active probes

active


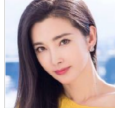






	SBI	Face artifacts	CNN detection	LRNet
True	0.9130 	0.0 	0.0 	0.81 
Fake	0.6507 	0.0 	0.0 	0.80 



Figure 3: Comparison of SBI, Face artifacts, CNN detection, and LRNet for true and fake faces.

Figure 4: Comparison of SBI, Face artifacts, CNN detection, and LRNet for true and fake faces.

Figure 5: Comparison of SBI, Face artifacts, CNN detection, and LRNet for true and fake faces.

Figure 6: Comparison of SBI, Face artifacts, CNN detection, and LRNet for true and fake faces.

Figure 7: Comparison of SBI, Face artifacts, CNN detection, and LRNet for true and fake faces.

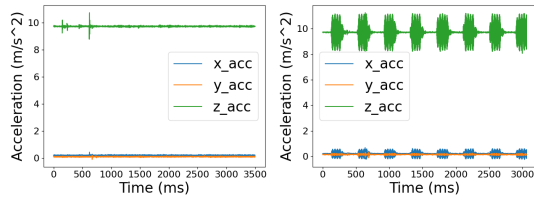
Figure 8: Comparison of SBI, Face artifacts, CNN detection, and LRNet for true and fake faces.

2.3. Intuition of Our Method

The intuition of our method is based on the observation that the real face and the fake face have different characteristics. The real face is more natural and has more consistent features, while the fake face is more artificial and has more inconsistencies. Our method aims to detect these inconsistencies and identify the fake face.

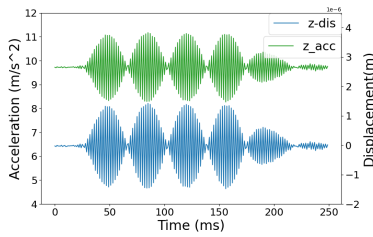
2.4. Related Smartphone Components

“Vibration” sound effect. The vibration sound effect is a common feature of smartphones. It is used to provide feedback to the user when they interact with the device. In our method, we use the vibration sound effect to create a fake face. The vibration sound effect is used to create a fake face that is more natural and has more consistent features.



(a)

(b)



(c)

Refocusing of the camera.

Refocusing of the camera.

Refocusing of the camera.

3. Feasibility Analysis

3.1. Induce Movement to Smartphone

Induce movement to smartphone.

3.1. Induce Movement to Smartphone

Induce movement to smartphone.

Induce movement to smartphone.

Induce movement to smartphone.

$$\begin{cases} V_{i+1} = V_i + a_i * \Delta t \\ D_{i+1} = D_i + V_i * \Delta t \\ D_0 = V_0 = 0 \end{cases} \quad (1)$$

Induce movement to smartphone.

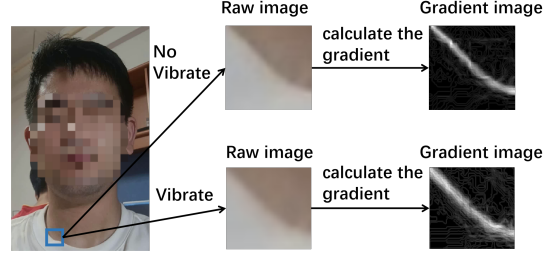
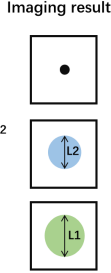
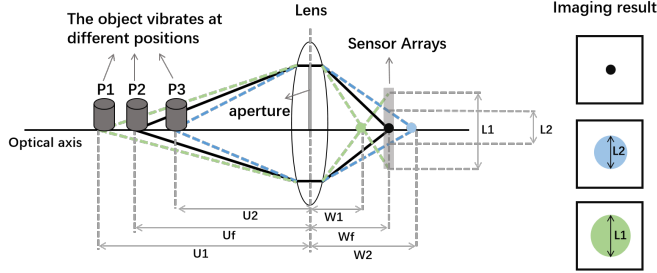
Induce movement to smartphone.

3.2. Induce Blur to Video

The structure of the camera and the blurriness under ideal conditions.

Induce blur to video.

Induce blur to video.



The object vibrates at different positions

Optical axis

The theoretical analysis of blurriness induced by vibration.

$$\frac{1}{f} = \frac{1}{w} + \frac{1}{u} \Rightarrow w = \frac{f * u}{u - f}, u = \frac{f * w}{w - f} \quad (2)$$

When the object vibrates, the image on the sensor array will be blurred.

$$\frac{w_2 - w_f}{L_2} = \frac{w_2}{F} \Rightarrow w_2 = \frac{f * w_f}{f - F * L_2} \quad (3)$$

$$\begin{cases} w_f = \frac{f * u_f}{u_f - f} \\ u_2 = \frac{f * w_2}{w_2 - f} \\ w_2 = \frac{f * w_f}{f - F * L_2} \end{cases} \quad (4)$$

When the object vibrates, the image on the sensor array will be blurred.

Imaging result

$$L_2 = \frac{f^2 * (u - u_2)}{F * (u - f) * u_2} \quad (5)$$

When the object vibrates, the image on the sensor array will be blurred.

$$L_1 = \frac{f^2 * (u_1 - u)}{F * (u - f) * u_1} \quad (6)$$

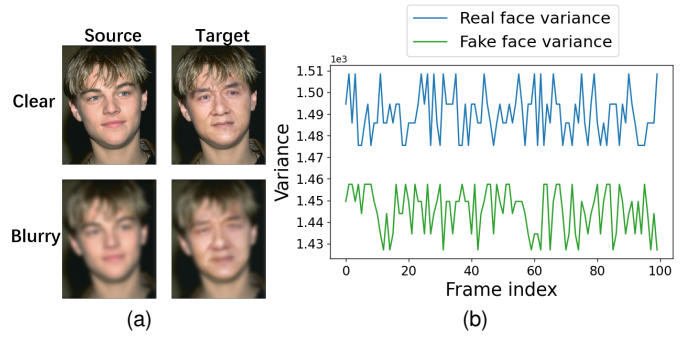
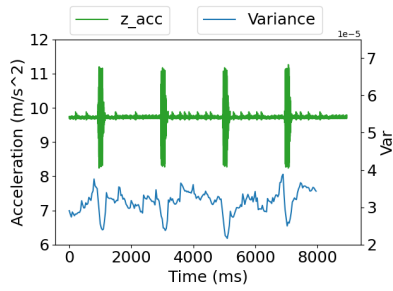
When the object vibrates, the image on the sensor array will be blurred.

Experimental parameters: $f = 1.8 \text{ cm}$, $u = 10 \text{ cm}$, $u_1 = 10 \text{ cm} + 1.5 \mu\text{m}$, $u_2 = 10 \text{ cm} - 1.5 \mu\text{m}$.
 Calculated values: $L_1 = 0.5 \text{ cm}$, $L_2 = 0.5 \text{ cm}$.

When the object vibrates, the image on the sensor array will be blurred.

The experimental verification of blurriness induced by vibration.

When the object vibrates, the image on the sensor array will be blurred.



Subplots

How deepfake algorithm deals with blurriness.

$$\sigma^2 = \frac{1}{N} \sum_{i=1}^N (x_i - \mu)^2 \quad (7)$$

How deepfake algorithm deals with blurriness.

μ

Subplots

How deepfake algorithm deals with blurriness.

4. System Design

How deepfake algorithm deals with blurriness.

How deepfake algorithm deals with blurriness.

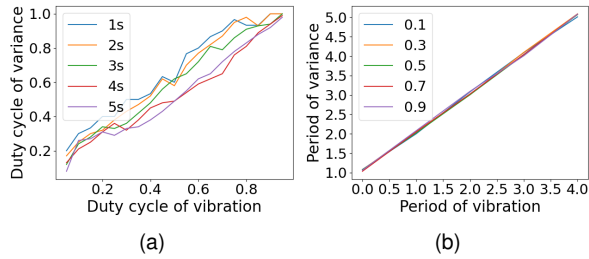
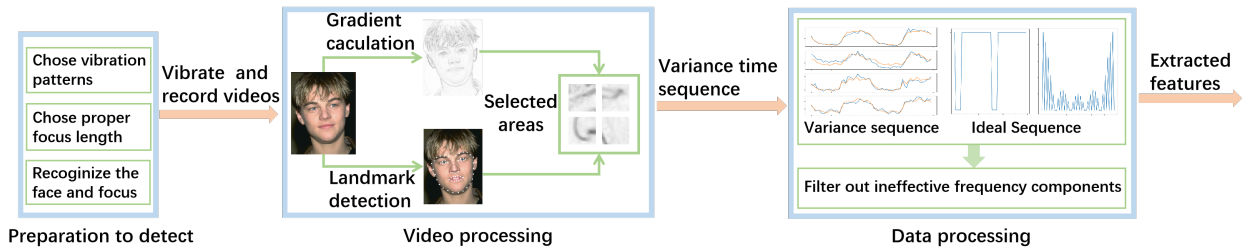
How deepfake algorithm deals with blurriness.

How deepfake algorithm deals with blurriness.

4.1. Preparation to Detection

Selection of vibration patterns.

Selection of vibration patterns.



1. (a) Duty cycle of variance vs. Duty cycle of vibration for different vibration periods.

2. (b) Period of variance vs. Period of vibration for different duty cycles.

3. Camera related preparation

4. VibrationEffect

5. Camera related preparation

6. Gradient calculation

4.2. Video Processing

7. Gradient calculation

8. Gradient calculation

9. Gradient calculation

10. Gradient calculation

11. Gradient calculation

12. Gradient calculation

13. Gradient calculation

14. Gradient calculation

15. Gradient calculation

16. Gradient calculation

17. Gradient calculation

18. Gradient calculation

19. Gradient calculation

20. Gradient calculation

21. Gradient calculation

22. Gradient calculation

23. Gradient calculation

24. Gradient calculation

$$g[i, j] = \frac{1}{9} \sum_{u=i-1}^{i+1} \sum_{v=j-1}^{j+1} abs(f[u, v] - f[i, j]) \quad (8)$$

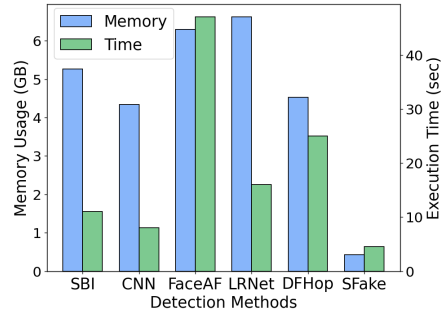
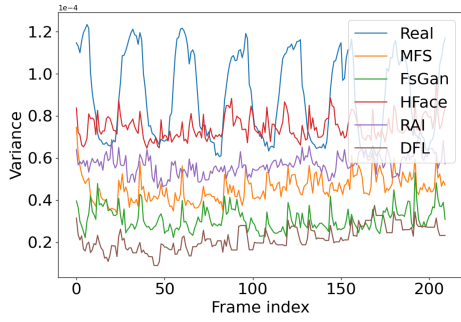
25. Gradient calculation

26. Gradient calculation

27. Gradient calculation

28. Gradient calculation

29. Gradient calculation



$\frac{1}{N} \sum_{i=1}^N \text{var}(f_{i, \text{real}})$
 $\frac{1}{N} \sum_{i=1}^N \text{var}(f_{i, \text{fake}})$
 $\frac{1}{N} \sum_{i=1}^N \text{var}(f_{i, \text{real}})$
 $\frac{1}{N} \sum_{i=1}^N \text{var}(f_{i, \text{fake}})$

$\frac{1}{N} \sum_{i=1}^N \text{var}(f_{i, \text{real}})$
 $\frac{1}{N} \sum_{i=1}^N \text{var}(f_{i, \text{fake}})$
 $\frac{1}{N} \sum_{i=1}^N \text{var}(f_{i, \text{real}})$
 $\frac{1}{N} \sum_{i=1}^N \text{var}(f_{i, \text{fake}})$

$\frac{1}{N} \sum_{i=1}^N \text{var}(f_{i, \text{real}})$
 $\frac{1}{N} \sum_{i=1}^N \text{var}(f_{i, \text{fake}})$
 $\frac{1}{N} \sum_{i=1}^N \text{var}(f_{i, \text{real}})$
 $\frac{1}{N} \sum_{i=1}^N \text{var}(f_{i, \text{fake}})$

$\frac{1}{N} \sum_{i=1}^N \text{var}(f_{i, \text{real}})$
 $\frac{1}{N} \sum_{i=1}^N \text{var}(f_{i, \text{fake}})$
 $\frac{1}{N} \sum_{i=1}^N \text{var}(f_{i, \text{real}})$
 $\frac{1}{N} \sum_{i=1}^N \text{var}(f_{i, \text{fake}})$

$\frac{1}{N} \sum_{i=1}^N \text{var}(f_{i, \text{real}})$
 $\frac{1}{N} \sum_{i=1}^N \text{var}(f_{i, \text{fake}})$
 $\frac{1}{N} \sum_{i=1}^N \text{var}(f_{i, \text{real}})$
 $\frac{1}{N} \sum_{i=1}^N \text{var}(f_{i, \text{fake}})$

5.2.2. Computation Performance.

We compare the computation performance of the proposed method with the baseline methods. The computation time is measured in terms of the number of floating-point operations (FLOPs) and the execution time. The execution time is measured in terms of the number of seconds. The FLOPs are measured in terms of the number of operations. The execution time is measured in terms of the number of seconds.

pmam -

$\frac{1}{N} \sum_{i=1}^N \text{var}(f_{i, \text{real}})$
 $\frac{1}{N} \sum_{i=1}^N \text{var}(f_{i, \text{fake}})$

$\frac{1}{N} \sum_{i=1}^N \text{var}(f_{i, \text{real}})$
 $\frac{1}{N} \sum_{i=1}^N \text{var}(f_{i, \text{fake}})$
 $\frac{1}{N} \sum_{i=1}^N \text{var}(f_{i, \text{real}})$
 $\frac{1}{N} \sum_{i=1}^N \text{var}(f_{i, \text{fake}})$

5.3. Impact Factors

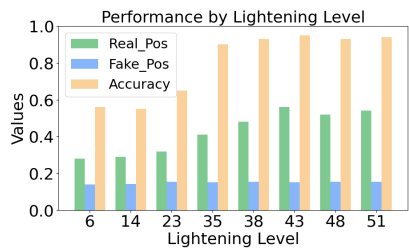
We analyze the impact of different factors on the performance of the proposed method. The factors include the number of frames, the number of features, and the number of layers. We analyze the impact of these factors on the performance of the proposed method.

Metrics and setup. Table 6

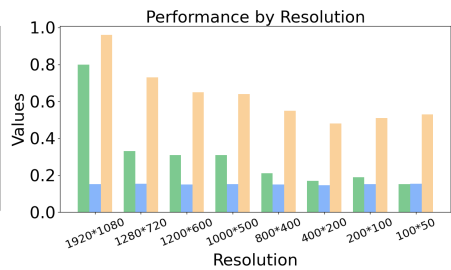
We compare the performance of the proposed method with the baseline methods. The performance is measured in terms of the accuracy and the execution time. The accuracy is measured in terms of the percentage of correct classifications. The execution time is measured in terms of the number of seconds.

$$POS = \frac{\sum(f_{avs}[\text{where } f_{ivs} \neq 0])}{\sum(f_{avs})} \quad (9)$$

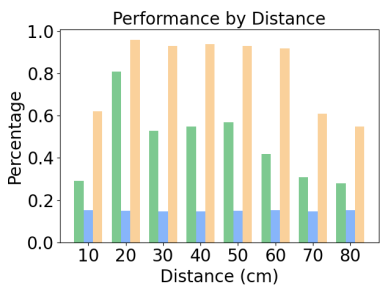
$\frac{1}{N} \sum_{i=1}^N \text{var}(f_{i, \text{real}})$
 $\frac{1}{N} \sum_{i=1}^N \text{var}(f_{i, \text{fake}})$
 $\frac{1}{N} \sum_{i=1}^N \text{var}(f_{i, \text{real}})$
 $\frac{1}{N} \sum_{i=1}^N \text{var}(f_{i, \text{fake}})$



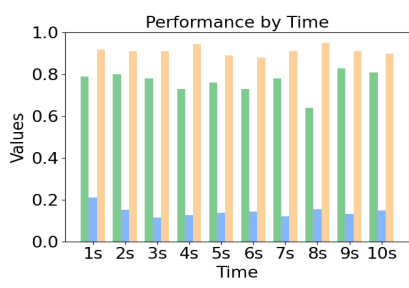
(a)



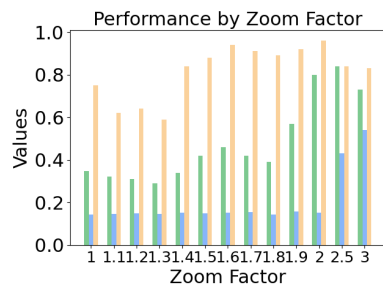
(b)



(c)



(d)



(e)

5.3.1. Lightning Level. `cv2.cvtColor`

```

img = cv2.cvtColor(img, cv2.COLOR_BGR2GRAY)
img = cv2.GaussianBlur(img, (5, 5), 0)
img = cv2.Canny(img, 1, 3)
img = cv2.dilate(img, np.ones((3, 3), dtype=np.uint8))
img = cv2.erode(img, np.ones((3, 3), dtype=np.uint8))

```

5.3.1. Lightning Level. `cv2.cvtColor`

```

img = cv2.cvtColor(img, cv2.COLOR_BGR2GRAY)
img = cv2.GaussianBlur(img, (5, 5), 0)
img = cv2.Canny(img, 1, 3)
img = cv2.dilate(img, np.ones((3, 3), dtype=np.uint8))
img = cv2.erode(img, np.ones((3, 3), dtype=np.uint8))

```

5.3.2. Resolution. `cv2.resize`

```

img = cv2.resize(img, (width, height))

```

`cv2.resize`

5.3.3. Shooting distance. `cv2.cvtColor`

```

img = cv2.cvtColor(img, cv2.COLOR_BGR2GRAY)
img = cv2.GaussianBlur(img, (5, 5), 0)
img = cv2.Canny(img, 1, 3)
img = cv2.dilate(img, np.ones((3, 3), dtype=np.uint8))
img = cv2.erode(img, np.ones((3, 3), dtype=np.uint8))

```

5.3.3. Shooting distance. `cv2.cvtColor`

```

img = cv2.cvtColor(img, cv2.COLOR_BGR2GRAY)
img = cv2.GaussianBlur(img, (5, 5), 0)
img = cv2.Canny(img, 1, 3)
img = cv2.dilate(img, np.ones((3, 3), dtype=np.uint8))
img = cv2.erode(img, np.ones((3, 3), dtype=np.uint8))

```

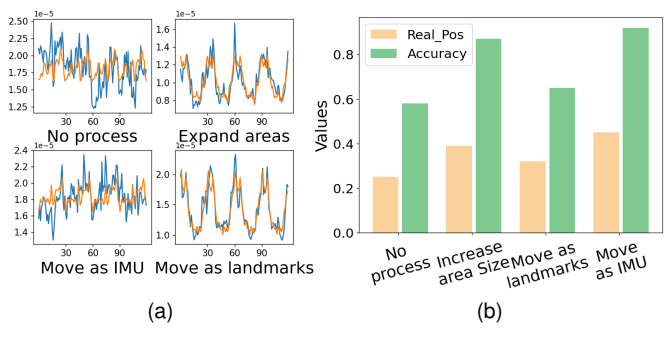



Fig. 3. Performance comparison of different methods.

is the probability of the selected area being updated. The value of p is set to 0.05. The value of f is set to 0.05.

Move the selected area by IMU data. The

area is updated by the IMU data. The value of p is set to 0.05. The value of f is set to 0.05.

$$p = \frac{d}{D} * f \quad (9)$$

d is the distance between the selected area and the centroid of landmarks.
 D is the diameter of the selected area.

is the probability of the selected area being updated. The value of p is set to 0.05. The value of f is set to 0.05. The value of d is set to 0.05. The value of D is set to 0.05.

Move the selected area by centroid of landmarks.

The area is updated by the centroid of landmarks. The value of p is set to 0.05. The value of f is set to 0.05.

is the probability of the selected area being updated. The value of p is set to 0.05. The value of f is set to 0.05.

6. Related Work

There are many methods for robot localization. The most common methods are particle filter [1], extended Kalman filter [2], and Monte Carlo localization [3]. In this paper, we propose a new method for robot localization based on the particle filter. The proposed method is more accurate and robust than the other methods.

7. Conclusion

In this paper, we proposed a new method for robot localization based on the particle filter. The proposed method is more accurate and robust than the other methods. The proposed method can be used in many applications.

Acknowledgments

References

[1] ...

P. Han, S. Kim, and S. Yoon, "A deep learning-based approach for detecting adversarial perturbations in face images," *Proc. of the 26th IEEE ICIP*, pp. 1-6, 2017.

S. Kim, S. Yoon, and P. Han, "A deep learning-based approach for detecting adversarial perturbations in face images," *Proc. of the 34th IEEE/CVF CVPR*, pp. 1-6, 2021.

S. Kim, S. Yoon, and P. Han, "A deep learning-based approach for detecting adversarial perturbations in face images," *Journal of Intelligent Engineering & Systems*, vol. 6, pp. 1-6, 2022.

S. Kim, S. Yoon, and P. Han, "A deep learning-based approach for detecting adversarial perturbations in face images," *Proc. of the 32nd IEEE/CVF CVPRW*, pp. 1-6, 2018.

S. Kim, S. Yoon, and P. Han, "A deep learning-based approach for detecting adversarial perturbations in face images," *Proc. of the 13th IEEE APSIPA ASC*, pp. 1-6, 2019.

S. Kim, S. Yoon, and P. Han, "A deep learning-based approach for detecting adversarial perturbations in face images," *Journal of Optometry*, vol. 10, pp. 1-6, 2023.

S. Kim, S. Yoon, and P. Han, "A deep learning-based approach for detecting adversarial perturbations in face images," *Pattern Recognition*, vol. 10, pp. 1-6, 2023.

S. Kim, S. Yoon, and P. Han, "A deep learning-based approach for detecting adversarial perturbations in face images," *Proc. of the 21st IEEE ICME*, pp. 1-6, 2020.

S. Kim, S. Yoon, and P. Han, "A deep learning-based approach for detecting adversarial perturbations in face images," *Advances in Neural Information Processing Systems*, vol. 34, pp. 1-6, 2021.

S. Kim, S. Yoon, and P. Han, "A deep learning-based approach for detecting adversarial perturbations in face images," *IEEE Trans. on Artificial Intelligence*, vol. 4, pp. 1-6, 2022.

S. Kim, S. Yoon, and P. Han, "A deep learning-based approach for detecting adversarial perturbations in face images," *Proc. of the 21st IEEE ICIP*, pp. 1-6, 2017.

S. Kim, S. Yoon, and P. Han, "A deep learning-based approach for detecting adversarial perturbations in face images," *Proc. of the 32nd IEEE/CVF CVPR*, pp. 1-6, 2018.

S. Kim, S. Yoon, and P. Han, "A deep learning-based approach for detecting adversarial perturbations in face images," *Journal of Metaverse*, vol. 1, pp. 1-6, 2023.

S. Kim, S. Yoon, and P. Han, "A deep learning-based approach for detecting adversarial perturbations in face images," *arXiv preprint arXiv:2006.07397*, 2020.

S. Kim, S. Yoon, and P. Han, "A deep learning-based approach for detecting adversarial perturbations in face images," *Proc. of the 36th IEEE/CVF CVPR*, pp. 1-6, 2023.

S. Kim, S. Yoon, and P. Han, "A deep learning-based approach for detecting adversarial perturbations in face images," *Proc. of the 33rd IEEE/CVF CVPR*, pp. 1-6, 2020.

S. Kim, S. Yoon, and P. Han, "A deep learning-based approach for detecting adversarial perturbations in face images," *IEEE Access*, vol. 10, pp. 1-6, 2022.

S. Kim, S. Yoon, and P. Han, "A deep learning-based approach for detecting adversarial perturbations in face images," *Proc. of the 35th IEEE/CVF CVPR*, pp. 1-6, 2022.

S. Kim, S. Yoon, and P. Han, "A deep learning-based approach for detecting adversarial perturbations in face images," *Proc. of the 43rd IEEE S&P*, pp. 1-6, 2023.

Proc. of the 2nd IEEE MIPR, 2019

Proc. of the 2nd IEEE MIPR, 2019

Proc. of the 16th ECCV, 2019

IEEE Trans. on Information Forensics and Security, 2020

ACM computing surveys (CSUR), 2020

Proc. of the 35th IEEE/CVF CVPR, 2020

Technology innovation management review, 2020

Transmission Electron Microscopy, 2020

Proc. of the 44th IEEE ICASSP, 2020

IEEE Transactions on Pattern Analysis and Machine Intelligence, 2020

arXiv preprint arXiv:2403.17881, 2020

IEEE Trans. on Information Forensics and Security, 2020

arXiv preprint arXiv:2007.08517, 2020

Proc. of the 16th ECCV, 2019

Proc. of the 34th IEEE/CVF CVPR, 2020

Proc. of the 32nd IEEE/CVF CVPR, 2019

Proc. of the 35th IEEE/CVF CVPR, 2020

Proc. of the 2nd IEEE ICTC, 2019

Real-Time Image Processing and Deep Learning 2019, 2019

Proc. of the 34th IEEE/CVF CVPR, 2020

Research Gate: Berlin, Germany, 2020

DeepFakes, 2020

Proc. of the 33rd IEEE/CVF CVPR, 2020

Proc. of the 37th AAAI, 2020

arXiv preprint arXiv:2106.09965, 2020

Proc. of the 36th AAAI, 2020

IEEE Trans. on Information Forensics and Security, 2020

Proc. of the 44th IEEE ICASSP, 2020

Proc. of the 15th ECCV, 2019

Iet Biometrics, 2020

Multimedia Tools and Applications, 2020

Proc. of the 30th IEEE/CVF CVPRW, 2020

Proc. of the 34th IEEE/CVF CVPR, 2020

Proc. of the 18th CVF/IEEE ICCV, 2019